Acta Cryst E CRYSTALLOGRAPHIC COMMUNICATIONS

ISSN 2056-9890

The 1:2 co-crystal formed between *N*,*N*′-bis-(pyridin-4-ylmethyl)ethanediamide and benzoic acid: crystal structure, Hirshfeld surface analysis and computational study

Sang Loon Tan and Edward R. T. Tiekink*

Research Centre for Crystalline Materials, School of Science and Technology, Sunway University, 47500 Bandar Sunway, Selangor Darul Ehsan, Malaysia. *Correspondence e-mail: edwardt@sunway.edu.my

Received 16 December 2019
Accepted 17 December 2019

Edited by W. T. A. Harrison, University of Aberdeen, Scotland

Keywords: crystal structure; oxalamide; hydrogen bonding; Hirshfeld surface analysis; computational chemistry.

CCDC reference: 1972449

Supporting information: this article has supporting information at journals.iucr.org/e

The crystal and molecular structures of the title 1:2 co-crystal, $C_{14}H_{14}N_4O_2\cdot 2C_7H_6O_2$, are described. The oxalamide molecule has a (+)-antiperiplanar conformation with the 4-pyridyl residues lying to either side of the central, almost planar $C_2N_2O_2$ chromophore (r.m.s. deviation = 0.0555 Å). The benzoic acid molecules have equivalent, close to planar conformations [C_6/CO_2 dihedral angle = 6.33 (14) and 3.43 (10)°]. The formation of hydroxy-O—H···N(pyridyl) hydrogen bonds between the benzoic acid molecules and the pyridyl residues of the diamide leads to a three-molecule aggregate. Centrosymmetrically related aggregates assemble into a six-molecule aggregate *via* amide-N—H···O(amide) hydrogen bonds through a 10-membered $\{\cdots HNC_2O\}_2$ synthon. These are linked into a supramolecular tape *via* amide-N—H···O(carbonyl) hydrogen bonds and 22-membered $\{\cdots HOCO\cdots NC_4NH\}_2$ synthons. The contacts between tapes to consolidate the three-dimensional architecture are of the type methylene-C—H···O(amide) and pyridyl-C—H···O(carbonyl). These interactions are largely electrostatic in nature. Additional non-covalent contacts are identified from an analysis of the calculated Hirshfeld surfaces.

1. Chemical context

Co-crystal technology continues to attract significant attention in a variety of endeavours with quite likely the most important of these relating to the development of more efficacious drugs by non-covalent derivatization of active pharmaceutical ingredients (Duggirala *et al.*, 2016; Bolla & Nangia, 2016; Gunawardana & Aakeröy, 2018). In order to predictably form co-crystals, reliable and robust synthons are needed. One such synthon is that formed by a carboxylic acid and a pyridyl residue *via* an O—H···N hydrogen bond (Shattock *et al.*, 2008). Very high propensities were noted, *i.e.* in the mid- to high-90%, in instances where there were no competing supramolecular synthons involving hydrogen bonding (Shattock *et al.*, 2008). This compares to 33% adoption of the more familiar eight-membered $\{\cdots OCOH\}_2$ homosynthon by carboxylic acids (Allen *et al.*, 1999). This high propensity for O—H···N hydrogen-bond formation pertains to bis(pyridin-*n*-ylmethyl)ethanediamide molecules, *i.e.* species with the general formula *n*-$NC_5H_4CH_2N(H)C(=O)C(=O)CH_2C_5H_4N$-*n*, for *n* = 2, 3 and 4, hereafter abbreviated as $^nLH_2$. Indeed, in early studies on crystal engineering, the combination of bifunctional $^nLH_2$ with dicarboxylic acids such as bis(carboxymethyl)-oxalamide (Nguyen *et al.*, 1998) and bis(carboxymethyl)urea (Nguyen *et al.*, 2001) enabled the systematic construction of two-dimensional arrays. As part of a long-term interest in the

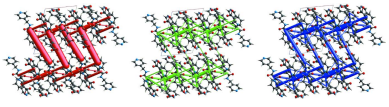

structural chemistry of $^{n}LH_2$ (Tiekink, 2017) and of systematic investigations of acid–pyridine co-crystals (Arman, Kaulgud *et al.*, 2012; Arman & Tiekink, 2013; Arman *et al.*, 2013, 2014), the title 1:2 co-crystal formed between $^{4}LH_2$ and benzoic acid was characterized by X-ray crystallography and the supramolecular association further probed by Hirshfeld surface analysis and computational chemistry.

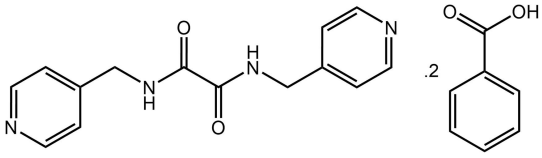

2. Structural commentary

The molecular structures of the three constituents comprising the crystallographic asymmetric unit of (I) are shown in Fig. 1. The $^{4}LH_2$ molecule lacks crystallographic symmetry but adopts a (+)-antiperiplanar conformation where the 4-pyridyl residues lie to either side of the central $C_2N_2O_2$ chromophore. The six atoms comprising the central residue are close to co-planar with their r.m.s. deviation equal to 0.0555 Å, with the maximum deviations to either side of the plane being 0.0719 (5) and 0.0642 (5) Å for the N2 and O2 atoms, respectively; the C6 and C9 atoms lie 0.1908 (14) and 0.0621 (14) Å out of and to one side of the plane (towards the N2 atom), respectively. The N1- and N4-pyridyl rings form dihedral angles of 86.00 (3) and 83.34 (2)°, respectively, with the plane through the $C_2N_2O_2$ atoms, so are close to perpendicular to the central plane. The dihedral angle between the pyridyl rings is 33.60 (5)°, indicating a splayed disposition as each pyridyl ring is folded away from the rest of the molecule. The carbonyl groups are *anti* and the molecule features intramolecular amide-N—H···O(carbonyl) hydrogen bonds that complete *S*(5) loops, Table 1.

There are two independent benzoic acid molecules in (I). Each is approximately planar with the dihedral angle between the benzene ring and CO_2 group being 6.33 (14) and 3.43 (10)° for the O3- and O5-benzoic acid molecules, respectively. As expected, the C15—O3(carbonyl) bond length of 1.2162 (13) Å is significantly shorter than the C15—O4(hydroxy) bond of 1.3197 (13) Å; the bonds of the O5-benzoic acid follow the same trend with C22—O5 of 1.2237 (13) Å compared with C22—O6 of 1.3084 (13) Å.

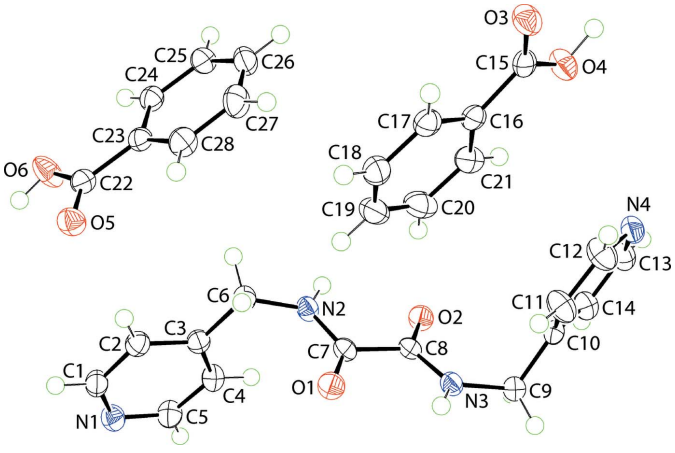

Figure 1
The molecular structures of the constituents of (I) showing the atom-labelling scheme and displacement ellipsoids at the 70% probability level.

Table 1
Hydrogen-bond geometry (Å, °).

D—H···*A*	*D*—H	H···*A*	*D*···*A*	*D*—H···*A*
N2—H2*N*···O2	0.88 (1)	2.36 (1)	2.7192 (12)	105 (1)
N3—H3*N*···O1	0.88 (1)	2.36 (1)	2.7154 (12)	104 (1)
O4—H4*O*···N1^{i}	0.86 (2)	1.78 (2)	2.6366 (12)	177 (2)
O6—H6*O*···N4^{ii}	0.86 (2)	1.72 (2)	2.5731 (13)	169 (2)
N2—H2*N*···O2^{iii}	0.88 (1)	2.05 (1)	2.8618 (12)	152 (1)
N3—H3*N*···O5^{iv}	0.88 (1)	2.12 (1)	2.8516 (12)	140 (1)
C1—H1···O3^{v}	0.95	2.58	3.2009 (14)	124
C2—H2···O5	0.95	2.47	3.3602 (14)	155
C6—H6*B*···O1^{iv}	0.99	2.41	3.3826 (14)	166
C12—H12···O3^{vi}	0.95	2.36	3.3025 (15)	171

Symmetry codes: (i) $x+1, y+1, z+1$; (ii) $x-1, y, z-1$; (iii) $-x+1, -y+1, -z+1$; (iv) $-x, -y+1, -z+1$; (v) $x-1, y-1, z-1$; (vi) $-x+1, -y+2, -z+2$.

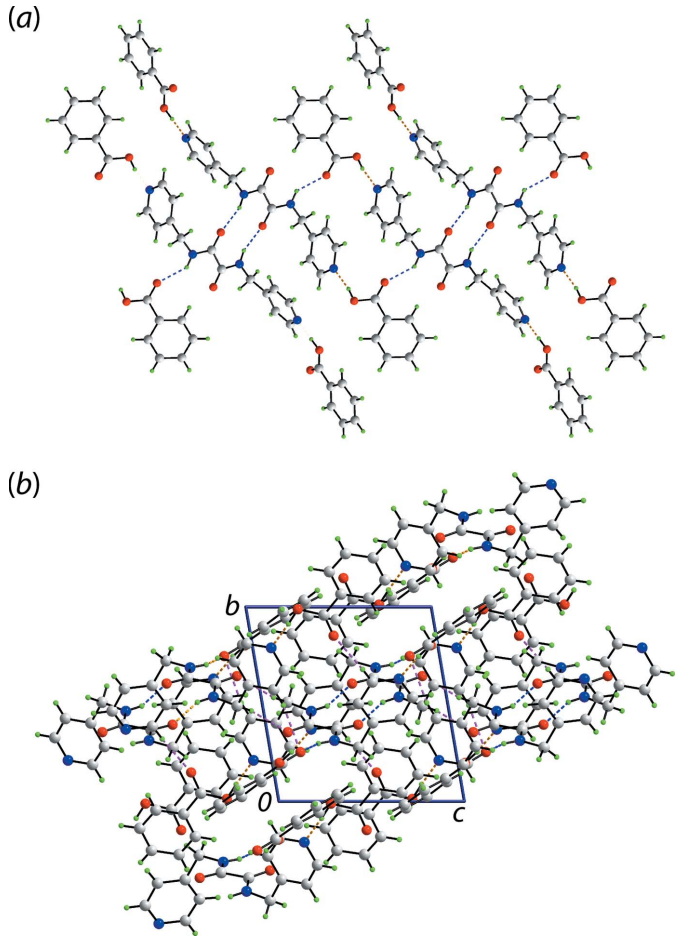

Figure 2
Molecular packing in the crystal of (I): (*a*) supramolecular tape sustained by hydroxy-O—H···N(pyridyl) (orange dashed lines) and amide-N—H···O(amide, carbonyl) hydrogen bonds and (*b*) a view of the unit-cell contents in projection down the *c* axis with C—H···O interactions shown as pink dashed lines.

3. Supramolecular features

As anticipated from the chemical composition, significant conventional hydrogen bonding is noted in the crystal of (I) over and above the intramolecular amide-N—H···O(carbonyl) hydrogen bonds already noted. The geometric parameters characterizing the specified intermolecular contacts are listed in Table 1. The most prominent feature in the crystal is the formation of the expected three-molecule aggregate sustained by hydroxy-O—H···N(pyridyl) hydrogen bonding. This is connected into a six-molecule aggregate *via* amide-N—H···O(amide) hydrogen bonding, which leads to a centrosymmetric ten-membered $\{\cdots HNC_2O\}_2$ synthon. The second amide forms an amide-N—H···O(carbonyl) bond with the result of that adjacent six-molecule aggregates are connected into a supramolecular tape *via* 22-membered $\{\cdots HOCO\cdots NC_4NH\}_2$ synthons, Fig. 2(*a*). The other notable contact within the tape is a pyridyl-C—H···O(carbonyl) interaction, which cooperates with a hydroxy-O—H···N(pyridyl) hydrogen bond to form a seven-membered {···OCOH···NCH} pseudo-heterosynthon; no analogous interaction is noted for the O5-benzoic acid. The supramolecular tapes are aligned along the *c*-axis direction and have a linear topology.

The connections between chains leading to a three-dimensional architecture are of the type C—H···O, *i.e.* methylene-C—H···O(amide) and pyridyl-C—H···O(carbonyl), the latter involving both pyridyl rings and each carbonyl-O atom, Table 1 and Fig. 2(*b*).

4. Hirshfeld surface analysis

The program *Crystal Explorer 17* (Turner *et al.*, 2017) was used for the calculation of the Hirshfeld surfaces and two-dimensional fingerprint plots based on the procedures described previously (Tan, Jotani *et al.*, 2019). The three-molecule aggregate whereby the two benzoic acid (BA) molecules are connected to $^4LH_2$ *via* the hydroxy-O—H···N(pyridyl) hydrogen bonds was used as the input for calculations. A list of the short interatomic contacts discussed below is given in Table 2. Through this analysis, several red spots were identified on the d_{norm} surfaces, Fig. 3, of the individual $^4LH_2$ and BA molecules, hereafter BA-I for the O3-containing molecule and BA-II for the O5-molecule, which indicate the presence of close contacts with distances shorter than the sum of the respective van der Waals radii (Spackman & Jayatilaka, 2009). Among all contacts, the terminal benzoic acid-O4—H4*O*···N1(pyridyl), benzoic acid-O6—H6*O*···N4(pyridyl), amide-N2—H2*N*···O2(amide) and amide-N3—H3*N*···O5(carbonyl) hydrogen-bonding interactions exhibit the most intense red spots on the d_{norm} surfaces, suggestive of strong interactions.

Other, relatively less intense red spots in Fig. 3(*a*) and (*b*) [in the order of moderate intensity (*m*) to weak intensity (*w*)] were identified for C6—H6*B*···O1 (*m*), C12—H12···O3 (*m*), C2—H2···O5 (*m*) and C1—H1···O3 (*w*), Table 1, and C20—H20···C8 (*m*), C28—H28···O1 (*w*), C9—H9*B*···C17 (*w*), C9—H9*B*···O3 (*w*), C13—H13···C1 (*w*), C12···C21 (*w*) and C8···C26 (*w*), Table 2. With the exception of the moderately

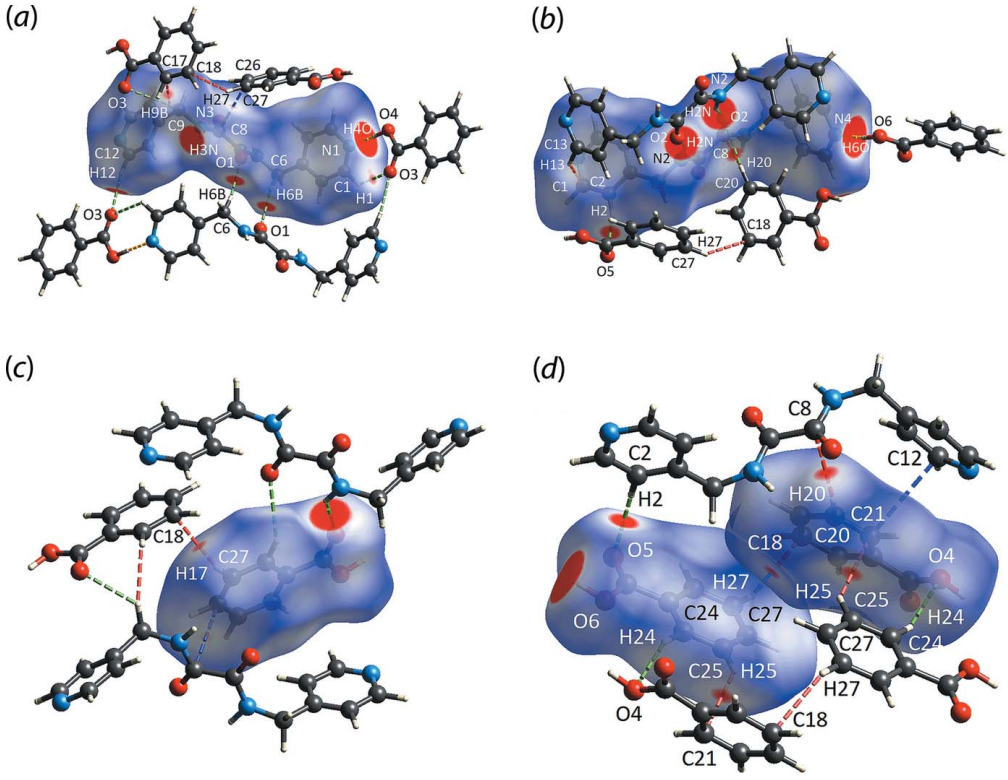

Figure 3
The d_{norm} map showing N—H···O (yellow dashed line), C—H···O (green), C—H···C (red) and C···C (blue) close contacts as indicated by the corresponding red spots with varying intensities within the range of −0.1004 to 1.1803 arbitrary units for (*a*) $^4LH_2$, (*b*) $^4LH_2$ viewed from a different perspective, (*c*) BA-II and (*d*) BA-II (left) and BA-I (right).

Table 2
A summary of short interatomic contacts (Å) in (I)[a].

Contact	Distance	Symmetry operation
O2···H2*N*[b]	1.94	$1-x, 1-y, 1-z$
C1···H13	2.79	$-1+x, y, -1+z$
N1···H4*O*[b]	1.65	$-1+x, -1+y, -1+z$
O3···H1	2.50	$1+x, 1+y, 1+z$
N4···H6*O*[b]	1.60	$1+x, y, 1+z$
O5···H3*N*[b]	2.02	$-x, 1-y, 1-z$
O1···H28	2.57	$-x, 1-y, 1-z$
O1···H6*B*	2.32	$-x, 1-y, 1-z$
C8···H20	2.61	x, y, z
C12···C21	3.39	x, y, z
C8···C26	3.35	$x, -1+y, z$
O5···H2	2.35	x, y, z
O3···H9*B*	2.56	$x, 1+y, z$
C17···H9*B*	2.69	$x, 1+y, z$
O3···H12	2.23	$1-x, 2-y, 2-z$
C21···H25	2.62	$1-x, 2-y, 1-z$
C18···H27	2.67	x, y, z
O4···H24	2.58	$1-x, 2-y, 1-z$

Notes: (*a*) The interatomic distances are calculated in *Crystal Explorer 17* (Turner *et al.*, 2017) whereby the *X*—H bond lengths are adjusted to their neutron values; (*b*) these interactions correspond to conventional hydrogen bonds.

intense red spot observed for C20—H20···C8 as well as those with relatively weak intensity, the other contacts are consistent with the interactions detected through an analysis with *PLATON* (Spek, 2020). As for the two benzoic acid molecules in the asymmetric unit, the contacts between them are established through C25—H25···C21, C27—H27···C18 as well as C24—H24···O4 interactions with diminutive intensity on the $d_{\rm norm}$ maps shown in Fig. 3(*c*) and (*d*).

The electrostatic potential mapping was performed on the individual $^4L\mathrm{H}_2$, BA-I and BA-II molecules through DFT-B3LYP/6-31G(*d*,*p*) to further study the nature of the close contacts, Fig. 4. The results are consistent with the above in that the O-–H···N and N—H···O hydrogen-bonding contacts that exhibited the most intense red spots on the $d_{\rm norm}$ map are highly electrostatic in nature, as evidenced from the intense electronegative (red) and electropositive (blue) regions on the Hirshfeld surfaces of the individual molecules. Other regions are relatively pale, indicating the complementary role of the remaining contacts in sustaining the molecular network in the crystal.

The two-dimensional fingerprint plots were generated in order to quantify the close contacts for compound (I) overall, *i.e.* the three-molecule aggregate specified above, as well as its individual $^4L\mathrm{H}_2$, BA-I and BA-II components, Fig. 5. The overall fingerprint plot of (I) exhibits a shield-like profile with a pair of symmetric spikes and contrasts those for the individual components with asymmetric spikes, indicating the interdependency between $^4L\mathrm{H}_2$ and benzoic acid in constructing the molecular packing of the system, in contrast to the previously reported benzene monosolvate of $^4L\mathrm{H}_2$ (Tan, Halcovitch *et al.*, 2019).

The major surface contacts for (I) can be split four ways: into H···H (38.0%), C···H/H···C (27.5%), O···H/H···O (25.2%) and N···H/H···N (3.5%) contacts. The distributions for H···H and N···H/H···N are evenly distributed between the internal (*i.e.* the donor or acceptor atoms internal to the surface) and external (*i.e.* the donor or acceptor atoms external to the surface) contacts. In contrast, for H···C/C···H and H···O/O···H, the distributions are slightly inclined towards (internal)-C···H-(external) (15.8%) and (internal)-O···H-(external) (13.4%) as compared to the corresponding

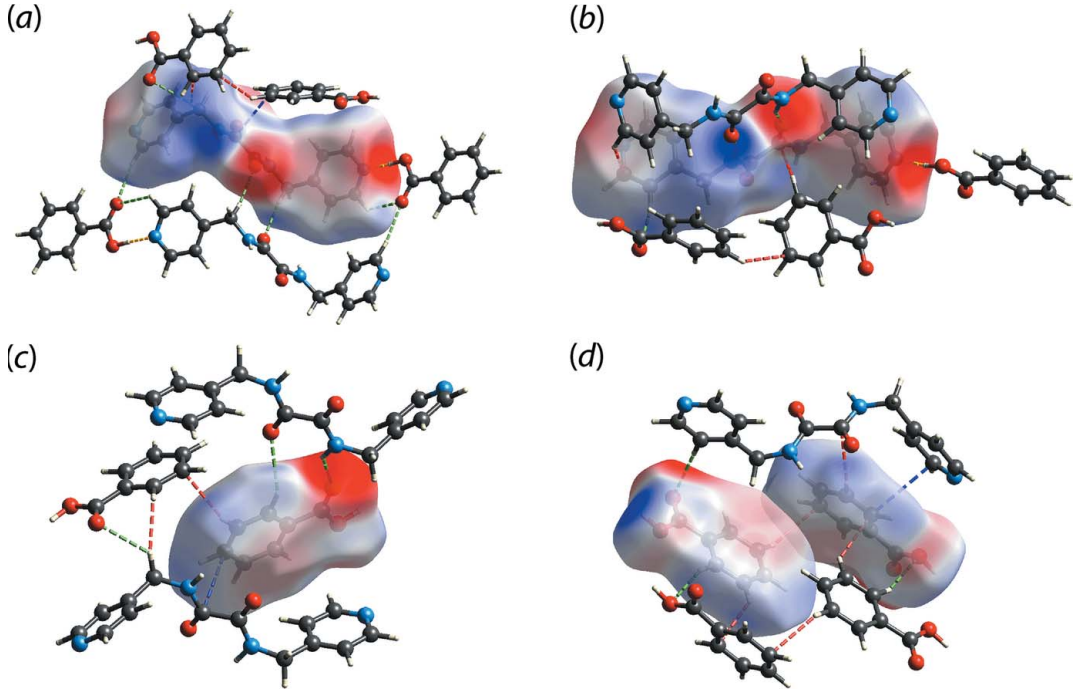

Figure 4
The electrostatic potential mapped onto the Hirshfeld surface within the isosurface range of −0.0562 to 0.0861 atomic units for (*a*) $^4L\mathrm{H}_2$, (*b*) $^4L\mathrm{H}_2$, (*c*) BA-II and (*d*) BA-II (left) and BA-I (right).

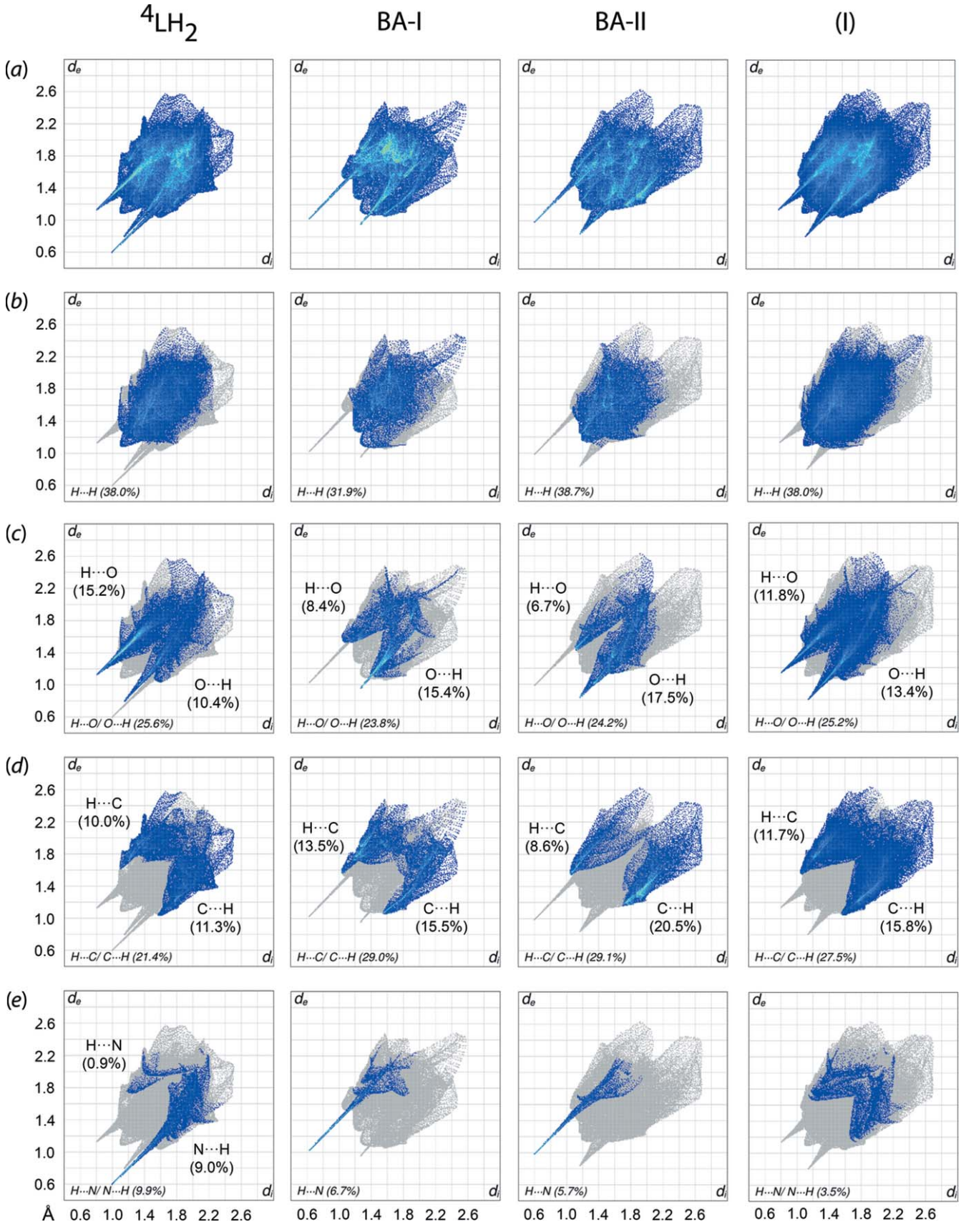

Figure 5
(*a*) The overall two-dimensional fingerprint plots for $^4LH_2$, BA-I, BA-II and the three-molecule aggregate in (I), and those delineated into (*b*) H···H, (*c*) H···O/O···H, (*d*) H···C/C···H and (*e*) H···N/N···H contacts, with the percentage contributions specified in each plot.

Table 3
A summary of interaction energies (kJ mol^{-1}) calculated for (I).

Contact	E_{ele}	E_{pol}	E_{dis}	E_{rep}	E_{tot}	Symmetry operation
N2—H2*N*···O2/						
C13—H13···C1	−60.9	−14.6	−58.5	82.5	−75.2	$1-x, 1-y, 1-z$
O4—H4*O*···N1/						
C1—H1···O3	−90.7	−21.3	−13.0	118.0	−50.1	$-1+x, -1+y, -1+z$
O6—H6*O*···N4	−95.2	−22.2	−11.3	134.4	−43.9	$1+x, y, 1+z$
N3—H3*N*···O5/						
C28—H28···O1	−32.8	−8.6	−16.1	30.3	−36.3	$-x, 1-y, 1-z$
C6—H6*B*···O1	−11.4	−5.1	−29.5	26.4	−25.1	$-x, 1-y, 1-z$
C20—H20···C8/						
C12···C21	−5.8	−1.5	−32.7	23.8	−21.0	x, y, z
C8···C26	−3.7	−1.0	−31.9	21.1	−19.4	$x, -1+y, z$
C2—H2···O5	−9.4	−1.9	−14.0	12.9	−15.6	x, y, z
C9—H9*B*···O3/						
C9—H9*B*···C17	−6.0	−2.2	−17.3	13.5	−14.7	$x, 1+y, z$
C12—H12···O3	−9.5	−2.4	−4.9	12.6	−8.3	$1-x, 2-y, 2-z$

counterparts at 11.7 and 11.8%, respectively. A detailed analysis of the $d_i + d_e$ distances shows that the closest H···O/O···H and H···C/C···H contacts of ∼1.95 Å and ∼2.62 Å, respectively, occur at distances shorter than the sum of the respective van der Waals radii of 2.61 and 2.79 Å, while the H···H (∼2.20 Å) and N···H/ H···N (2.80 Å) contacts are longer than the sum of van der Waals radii of 2.18 and 2.64 Å, respectively.

The $^4LH_2$ molecule also displays a shield-like profile with asymmetric spikes which upon further decomposition could be delineated into H···H (38.0%), H···O/O···H (25.6%), H···C/C···H (21.4%) and H···N/N···H (9.9%) contacts. The H···O/O···H contact exhibits a forceps-like profile with the distribution inclined towards internal-H···O-external (15.2%) as compared to internal-O···H-external (10.4%), and both with tips at $d_i + d_e$ ∼1.94 Å which is indicative of significant hydrogen bonding. Similarly, the asymmetric, needle-like profile for the H···N/N···H contact is inclined towards the internal-N···H-external (9.0%) with the tip at $d_i + d_e$ = ∼1.6 Å, while the remaining 0.9% is attributed to the internal-H···N-external contact with $d_i + d_e$ of ∼2.94 Å (> sum of van der Waals radii). The H···C/C···H contacts are evenly distributed on both sides of the contacts with the $d_i + d_e$ of ∼2.64 Å which is slightly shorter than the sum of van der Waals radii. On the other hand, the H···H contacts have little direct influence in sustaining the molecular packing as shown from the shortest $d_i + d_e$ value of ∼2.2 Å, which is longer than the sum of the van der Waals radii despite the prominent contributions these make to the overall surface

As for the pair of BA molecules, both BA-I and BA-II possess similar, claw-like profiles which differ in the diffuse region, with the former being the characteristic of H···H contacts while the latter is due to H···C/C···H interactions. Quantitatively, differences mainly relate to the percentage contribution by H···H contacts, *i.e.* 31.9% for BA-I *cf.* 38.7% for BA-II. The discrepancy in the distribution for BA-I is compensated by the increase in O···C/C···O and C···C contacts with the distribution being 4.8 and 2.9%, respectively. The distribution for H···C/C···H (29.0 *vs* 29.1%), H···O/O···H (23.8 *vs* 24.2%) and H···N (6.7 *vs* 5.7%) contacts is approximately the same in both BA-I and BA-II, except that the H···C/C···H distribution for BA-II is significantly more inclined towards internal-C···H-external (20.5%) than the internal-H···C-external (8.6%) in contrast to the relatively balanced distribution for BA-I 15.5% for internal-C···H-external *vs* 13.5% for internal-H···C-external. In BA-I, the $d_i + d_e$ values for H···O/O···H, H···C/C···H and H···N/N···H at the tips are ∼2.26–2.70, 2.62 and 1.64 Å, respectively, while the equivalent values for the analogous contacts for BA-II have tips at 2.02–2.56, 2.62–2.86 and 1.58 Å, respectively. Among these contact distances, the O···H, H···C/C···H and H···N for BA-I as well as H···O/O···H, H···C and H···N for BA-II are shorter than the sum of van der Waals radii. As expected, the minimum $d_i + d_e$ value for the H···H contacts is longer than the sum of van der Waals radii, even if it is the most dominant contact for each molecule. The aforementioned data for BA-I and BA-II clearly distinguishes the independent molecules.

5. Computational chemistry

To assess the strength of the specified interactions in the Hirshfeld surface analysis, the molecules in (I) were subjected to energy calculations through *CrystalExplorer17* (Turner *et al.*, 2017); the results are collated in Table 3. Among all close contacts present in (I), the pairwise interactions of the amide-N2—H2*N*···O2(amide) hydrogen bonds complemented by a pair of pyridyl-C13—H13···C1(pyridyl) interactions between two oxamide molecules led to the greatest interaction energy (E_{tot}) of −75.2 kJ mol^{-1}. This value is comparable to E_{tot} of −71.7 kJ mol^{-1} calculated for the classical eight-membered {···HOCO}$_2$ interaction (Tan & Tiekink, 2019*a*). The second strongest interaction arises from the hydroxy-O4—H4*O*···N1(pyridyl) and pyridyl-C1—H1···O3(carbonyl) contacts, which combine to generate a seven-membered heterosynthon with E_{tot} of −50.1 kJ mol^{-1}. A diminution in E_{tot} is observed for the other pyridyl terminus, which only comprises a carboxylic-O6—H6*O*···N4(pyridyl) hydrogen bond without a supporting pyridyl-C—H···O(carbonyl)

Table 4
Selected geometric data, *i.e.* central C—C bond length, O—H···N and NC—H···O(carbonyl) separations (Å) for $^4LH_2$ in its co-crystals with carboxylic acids and salt with a carboxylate anion.

Carboxylic acid (CA)	Symmetry of $^4LH_2$	C—C	O—H···N(pyridyl)	NC—H···O(carbonyl)	REFCODE	Reference
1:1 co-crystal						
bis(carboxymethyl)urea	–	1.53 (2)	1.73	2.54	CAJRAH	Nguyen *et al.* (2001)
			1.75	4.21		
diglycineoxamide	$\bar{1}$	1.514 (5)	1.74	3.11	SEPSIP01	Nguyen *et al.* (2001)
poly(1,2-bis(2-carboxyethyl)-tetra-1-en-3-yn-1,4-diyl	$\bar{1}$	1.537 (13)	1.80	2.98	DOVSIR	Curtis *et al.* (2005)
2:1 co-crystal						
(4-nitrophenyl)acetic acid	$\bar{1}$	1.543 (2)	1.57	2.72	NAXMEG	Arman, Kaulgud *et al.* (2012)
benzoic acid	–	1.5401 (14)	1.67	2.59	–	This work
			1.72	3.46		
2-methylbenzoic acid	$\bar{1}$	1.5356 (19)	1.79	2.60	WADXUX	Syed *et al.* (2016)
acetic acid[a]	$\bar{1}$	1.5397 (17)	1.75	2.81	GOQQIP	Tan & Tiekink (2019*b*)
2-[(4-hydroxyphenyl)diazenyl]-benzoic acid[b]	$\bar{1}$	1.542 (2)	1.89	–	AJEZEV	Arman *et al.* (2009)
2,6-dinitrobenzoate[c]	$\bar{1}$	1.543 (3)	1.96[c]	2.51	TIPGUW	Arman, Miller *et al.* (2012)

Notes: (*a*) Characterized as a di-hydrate; (*b*) hydroxy-O—N(pyridyl) hydrogen bond; (*c*) salt with a pyridinium-N—H···O(carboxylate) hydrogen bond.

interaction, showing an energy of −43.9 kJ mol^{-1} and ranked third strongest among all interactions in (I).

The next highest interaction energy with E_{tot} of −36.3 kJ mol^{-1} involves contributions from the amide-N3—H3*N*···O5(carboxylic acid) and phenyl-C28—H28···O1(amide) contacts. Other interactions include the methylene-C6—H6*B*···O1(amide) contacts (–25.1 kJ mol^{-1}), the combination of benzoic acid-C20—H20···C8(amide) and benzoic acid-C12···C21(pyridyl) (–21.0 kJ mol^{-1}), amide-C8···C26(benzoic acid) (–19.4 kJ mol^{-1}), pyridyl-C2—H2···O5(carboxylic acid) (–15.6 kJ mol^{-1}), a combination of (pyridine methyl)-C9—H9*B*···O3(carboxylic acid) and methylene-C9—H9*B*···C17(benzoic acid) (−14.7 kJ mol^{-1}), as well as pyridyl-C12—H12···O3(carboxylic acid) (–8.3 kJ mol^{-1}). Some inconsistencies are observed between the calculated E_{tot} and Hirshfeld surface analysis, particularly for C2—H2···O5 and C12—H12···O3. These interactions can be considered weak even though they possess a relatively short contact distance compared to the sum of van der Waals radii, as indicated from the moderately intense red spots on the Hirshfeld surface. The contradiction could arise as a result of the relatively high repulsion terms, which weaken the interaction energy.

Overall, the crystal of (I) is mainly sustained by electrostatic forces owing to the strong ten-membered $\{\cdots HNC_2O\}_2$ synthon as well as the terminal interactions between $^4LN_2$ and BA molecules, through hydroxy-O—H4···N(pyridyl) hydrogen bonds, lead to a zigzag electrostatic energy framework, Fig. 6(*a*). The packing system is further stabilized by the dispersion forces contributed by the ten-membered $\{\cdots HNC_2O\}_2$ synthon complemented by other peripheral interactions such the pairwise C20—H20···C8/C12···C21, C8···C26 and C6—H6*B*···O1 interactions, which result in a dispersion energy framework resembling a spider web, Fig. 6(*b*). The combination of the electrostatic and dispersion forces leads to an overall energy framework that resembles a ladder, Fig. 6(*c*).

6. Database survey

As indicated in the *Chemical context*, $^4LH_2$ molecules have long been known to form co-crystals with carboxylic acids. A list of $^4LH_2$/carboxylic acid co-crystals is given in Table 4, highlighting the symmetry of $^4LH_2$, the length of the central C—C bond, recognized as being long (Tiekink, 2017; Tan & Tiekink, 2020), and the O—H···N and NC—H···O (involving

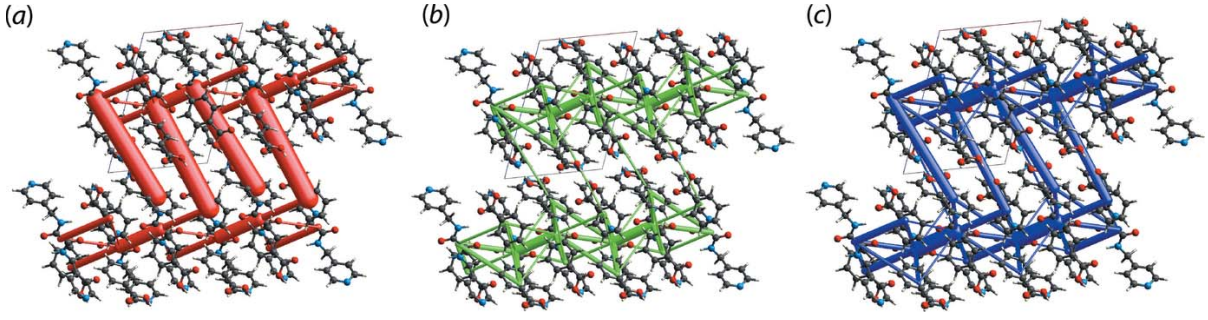

Figure 6
Perspective views of the energy frameworks of (I), showing the (*a*) electrostatic force, (*b*) dispersion force and (*c*) total energy. The cylindrical radius is proportional to the relative strength of the corresponding energies and they were adjusted to the same scale factor of 100 with a cut-off value of 8 kJ mol^{-1} within a 2 × 2 × 2 unit cells.

the C—H atom adjacent to the pyridyl-nitrogen atom) separations associated with the hydroxy-O—H···N(pyridyl) hydrogen bond. The data are separated into 1:1 and 1:2 $^4LH_2$:carboxylic acid species. In all cases, $^4LH_2$ adopts an anti-periplanar disposition of the pyridyl rings whereby the pyridyl rings lie to either side of the central $C_2N_2O_2$ chromophore; often this is crystallographically imposed. This matches the situation in the two known polymorphs of $^4LH_2$ (Lee & Wang, 2007; Lee, 2010), but contrasts with the conformational diversity found in the isomeric $^3LH_2$ molecules, *i.e.* in the polymorphs (Jotani *et al.*, 2016) and multi-component crystals (Tan & Tiekink, 2020). All but one structure forms hydroxyl-O—H···N(pyridyl) hydrogen bonds, involving both pyridyl rings, in their crystals. One reason put forward for the stability of hydroxy-O—H···N(pyridyl) hydrogen bonds is the close approach of the pyridyl-C—H and carbonyl-O atoms to form a seven-membered {···O=COH···NCH} pseudo-synthon. In most, but not all examples, the carboxylic acid and pyridyl ring approach co-planarity, enabling the formation of the aforementioned pseudo-synthon. Among the co-crystals, only one example does not form the anticipated hydroxyl-O—H···N(pyridyl) hydrogen bonds. In this case, the co-former, *i.e.* 2-[(4-hydroxyphenyl)diazenyl]benzoic acid, carries a hydroxyl residue and this preferentially forms the hydrogen bonds to the pyridyl-N atoms. This observation is contrary to literature expectation where the carboxylic acid would be expected to form hydrogen bonds preferentially to pyridyl-N atom in instances where there is a competition with putative hydroxyl-O—H···N(pyridyl) hydrogen bonds (Shattock *et al.*, 2008). In this structure, the carboxylic acid is able to form an intramolecular hydroxy-O—H···N(azo) hydrogen bond to close an *S*(6) loop, in accord with Etter's rules, *i.e.* '*six-membered ring intramolecular hydrogen bonds form in preference to intermolecular hydrogen bonds*' (Etter, 1990). Finally, and for completeness, details for a salt are included in Table 4. Here, proton transfer has occurred, leading to a pyridinium-N—H···O(carboxylate) hydrogen bond.

7. Synthesis and crystallization

The precursor, *N*,*N*′-bis(pyridin-4-ylmethyl)oxalamide ($^4LH_2$), was prepared according to the literature; M.p.: 486.3–487.6 K; lit. 486–487 K (Nguyen *et al.*, 1998). Reagent-grade benzoic acid (Merck) was used as received without further purification. Solid $^4LH_2$ (0.271 g, 0.001 mol) was mixed with benzoic acid (0.122 g, 0.001 mol) and the physical mixture was then ground for 15 min in the presence of a few drops of methanol. The procedures were repeated three times. Colourless blocks were obtained through careful layering of toluene (1 ml) on an *N*,*N*-dimethylformamide (1 ml) solution of the ground mixture. M.p.: 435.4–436 K. IR (cm^{-1}): 3321 ν(N—H), 3070–2999 ν(C—H), 1702–1662 ν(C=O), 1506 ν(C=C), 1417 ν(C—N).

Similar experiments with $^4LH_2$:benzoic acid in molar ratios of 1:2, 1:3 and 1:4 were also attempted but only the 2:1 co-crystal (I) was isolated after recrystallization of the powders.

Table 5
Experimental details.

Crystal data	
Chemical formula	$C_{14}H_{14}N_4O_2{\cdot}2C_7H_6O_2$
M_r	514.53
Crystal system, space group	Triclinic, $P\overline{1}$
Temperature (K)	100
a, b, c (Å)	9.6543 (2), 9.9235 (2), 14.1670 (3)
α, β, γ (°)	100.755 (2), 108.318 (2), 95.617 (2)
V (Å^3)	1247.90 (5)
Z	2
Radiation type	Cu $K\alpha$
μ (mm^{-1})	0.81
Crystal size (mm)	0.12 × 0.07 × 0.05
Data collection	
Diffractometer	Rigaku XtaLAB Synergy Dualflex AtlasS2
Absorption correction	Gaussian (*CrysAlis PRO*; Rigaku OD, 2018)
T_{min}, T_{max}	0.832, 1.000
No. of measured, independent and observed [$I > 2\sigma(I)$] reflections	31534, 5220, 4736
R_{int}	0.031
(sin $\theta/\lambda)_{max}$ (Å^{-1})	0.630
Refinement	
$R[F^2 > 2\sigma(F^2)]$, $wR(F^2)$, S	0.034, 0.093, 1.02
No. of reflections	5220
No. of parameters	359
No. of restraints	4
H-atom treatment	H atoms treated by a mixture of independent and constrained refinement
$\Delta\rho_{max}$, $\Delta\rho_{min}$ (e Å^{-3})	0.21, −0.28

Computer programs: *CrysAlis PRO* (Rigaku OD, 2018), *SHELXS* (Sheldrick, 2015*a*), *SHELXL2017/1* (Sheldrick, 2015*b*), *ORTEP-3 for Windows* (Farrugia, 2012), *DIAMOND* (Brandenburg, 2006) and *publCIF* (Westrip, 2010).

8. Refinement

Crystal data, data collection and structure refinement details are summarized in Table 5. The carbon-bound H atoms were placed in calculated positions (C—H = 0.95–0.99 Å) and were included in the refinement in the riding-model approximation, with U_{iso}(H) set to 1.2U_{eq}(C). The oxygen- and nitrogen-bound H atoms were located from a difference Fourier map and refined with O—H = 0.84±0.01 Å and N—H = 0.88±0.01 Å, respectively, and with U_{iso}(H) set to 1.5U_{eq}(O) or 1.2U_{eq}(N).

Funding information

Crystallographic research at Sunway University is supported by Sunway University Sdn Bhd (Grant no. STR-RCTR-RCCM-001-2019).

References

Allen, F. H., Motherwell, W. D. S., Raithby, P. R., Shields, G. P. & Taylor, R. (1999). *New J. Chem.* **23**, 25–34.
Arman, H. D., Kaulgud, T., Miller, T., Poplaukhin, P. & Tiekink, E. R. T. (2012). *J. Chem. Crystallogr.* **42**, 673–679.
Arman, H. D., Kaulgud, T., Miller, T. & Tiekink, E. R. T. (2014). *Z. Kristallogr. Cryst. Mater.* **229**, 295–302.
Arman, H. D., Miller, T., Poplaukhin, P. & Tiekink, E. R. T. (2009). *Acta Cryst.* E**65**, o3178–o3179.

Arman, H. D., Miller, T., Poplaukhin, P. & Tiekink, E. R. T. (2013). *Z. Kristallog.* **228**, 295–303.
Arman, H. D., Miller, T. & Tiekink, E. R. T. (2012). *Z. Kristallogr.* **227**, 825–830.
Arman, H. D. & Tiekink, E. R. T. (2013). *Zeitschrift für Kristallogr.* **228**, 289–294.
Bolla, G. & Nangia, A. (2016). *Chem. Commun.* **52**, 8342–8360.
Brandenburg, K. (2006). *DIAMOND*. Crystal Impact GbR, Bonn, Germany.
Curtis, S. M., Le, N., Nguyen, T., Ouyang, X., Tran, T., Fowler, F. W. & Lauher, J. W. (2005). *Supramol. Chem.* **17**, 31–36.
Duggirala, N. K., Perry, M. L., Almarsson, Ö. & Zaworotko, M. J. (2016). *Chem. Commun.* **52**, 640–655.
Etter, M. C. (1990). *Acc. Chem. Res.* **23**, 120–126.
Farrugia, L. J. (2012). *J. Appl. Cryst.* **45**, 849–854.
Gunawardana, C. A. & Aakeröy, C. B. (2018). *Chem. Commun.* **54**, 14047–14060.
Jotani, M. M., Zukerman-Schpector, J., Madureira, L. S., Poplaukhin, P., Arman, H. D., Miller, T. & Tiekink, E. R. T. (2016). *Z. Kristallogr. Cryst. Mater*. **231**, 415–425.
Lee, G.-H. (2010). *Acta Cryst.* C**66**, o241–o244.
Lee, G.-H. & Wang, H.-T. (2007). *Acta Cryst.* C**63**, m216–m219.
Nguyen, T. L., Fowler, F. W. & Lauher, J. W. (2001). *J. Am. Chem. Soc.* **123**, 11057–11064.
Nguyen, T. L., Scott, A., Dinkelmeyer, B., Fowler, F. W. & Lauher, J. W. (1998). *New J. Chem.* **22**, 129–135.
Rigaku OD (2018). *CrysAlis PRO* Software system. Rigaku Corporation, Oxford, UK.
Shattock, T. R., Arora, K. K., Vishweshwar, P. & Zaworotko, M. J. (2008). *Cryst. Growth Des.* **8**, 4533–4545.
Sheldrick, G. M. (2015*a*). *Acta Cryst.* A**71**, 3–8.
Sheldrick, G. M. (2015*b*). *Acta Cryst.* C**71**, 3–8.
Spackman, M. A. & Jayatilaka, D. (2009). *CrystEngComm*, **11**, 19–32.
Spek, A. L. (2020). *Acta Cryst.* E**76**, 1–11.
Syed, S., Jotani, M. M., Halim, S. N. A. & Tiekink, E. R. T. (2016). *Acta Cryst.* E**72**, 391–398.
Tan, S. L., Halcovitch, N. R. & Tiekink, E. R. T. (2019). *Acta Cryst.* E**75**, 1133–1139.
Tan, S. L., Jotani, M. M. & Tiekink, E. R. T. (2019). *Acta Cryst.* E**75**, 308–318.
Tan, S. L. & Tiekink, E. R. T. (2019*a*). *Acta Cryst.* E**75**, 1–7.
Tan, S. L. & Tiekink, E. R. T. (2019*b*). *Z. Kristallogr. New Cryst. Struct.* **234**, 1109–1111.
Tan, S. L. & Tiekink, E. R. T. (2020). *Acta Cryst.* E**76**, 25–31.
Tiekink, E. R. T. (2017). *Multi-Component Crystals: Synthesis, Concepts, Function*, edited by E. R. T. Tiekink & J. Schpector-Zukerman, pp. 289–319. De Gruyter: Singapore.
Turner, M. J., Mckinnon, J. J., Wolff, S. K., Grimwood, D. J., Spackman, P. R., Jayatilaka, D. & Spackman, M. A. (2017). *Crystal Explorer 17*. The University of Western Australia.
Westrip, S. P. (2010). *J. Appl. Cryst.* **43**, 920–925.

supporting information

Acta Cryst. (2020). E**76**, 102-110 [https://doi.org/10.1107/S2056989019016840]

The 1:2 co-crystal formed between *N*,*N*′-bis(pyridin-4-ylmethyl)ethanediamide and benzoic acid: crystal structure, Hirshfeld surface analysis and computational study

Sang Loon Tan and Edward R. T. Tiekink

Computing details

Data collection: *CrysAlis PRO* (Rigaku OD, 2018); cell refinement: *CrysAlis PRO* (Rigaku OD, 2018); data reduction: *CrysAlis PRO* (Rigaku OD, 2018); program(s) used to solve structure: *SHELXS* (Sheldrick, 2015*a*); program(s) used to refine structure: *SHELXL2017/1* (Sheldrick, 2015*b*); molecular graphics: *ORTEP-3 for Windows* (Farrugia, 2012), *DIAMOND* (Brandenburg, 2006); software used to prepare material for publication: *publCIF* (Westrip, 2010).

N,*N*′-bis(pyridin-4-ylmethyl)ethanediamide; bis(benzoic acid)

Crystal data

$C_{14}H_{14}N_4O_2{\cdot}2C_7H_6O_2$
M_r = 514.53
Triclinic, $P\overline{1}$
a = 9.6543 (2) Å
b = 9.9235 (2) Å
c = 14.1670 (3) Å
α = 100.755 (2)°
β = 108.318 (2)°
γ = 95.617 (2)°
V = 1247.90 (5) Å^3
Z = 2
$F(000)$ = 540
D_x = 1.369 Mg m^{-3}
Cu $K\alpha$ radiation, λ = 1.54184 Å
Cell parameters from 16947 reflections
θ = 3.3–76.2°
μ = 0.81 mm^{-1}
T = 100 K
Prism, colourless
0.12 × 0.07 × 0.05 mm

Data collection

Rigaku XtaLAB Synergy Dualflex AtlasS2 diffractometer
Radiation source: micro-focus sealed X-ray tube
Detector resolution: 5.2558 pixels mm^{-1}
ω scans
Absorption correction: gaussian (CrysAlis PRO; Rigaku OD, 2018)
T_{min} = 0.832, T_{max} = 1.000
31534 measured reflections
5220 independent reflections
4736 reflections with $I > 2\sigma(I)$
R_{int} = 0.031
θ_{max} = 76.4°, θ_{min} = 3.4°
h = −12→12
k = −12→12
l = −17→17

Refinement

Refinement on F^2
Least-squares matrix: full
$R[F^2 > 2\sigma(F^2)]$ = 0.034
$wR(F^2)$ = 0.093
S = 1.02
5220 reflections
359 parameters
4 restraints
Primary atom site location: structure-invariant direct methods
Secondary atom site location: difference Fourier map
Hydrogen site location: mixed

H atoms treated by a mixture of independent and constrained refinement
$w = 1/[\sigma^2(F_o^2) + (0.0539P)^2 + 0.3396P]$ where $P = (F_o^2 + 2F_c^2)/3$

$(\Delta/\sigma)_{max} = 0.001$
$\Delta\rho_{max} = 0.21$ e Å^{-3}
$\Delta\rho_{min} = -0.28$ e Å^{-3}

Special details

Geometry. All esds (except the esd in the dihedral angle between two l.s. planes) are estimated using the full covariance matrix. The cell esds are taken into account individually in the estimation of esds in distances, angles and torsion angles; correlations between esds in cell parameters are only used when they are defined by crystal symmetry. An approximate (isotropic) treatment of cell esds is used for estimating esds involving l.s. planes.

Fractional atomic coordinates and isotropic or equivalent isotropic displacement parameters (Å^2)

	x	*y*	*z*	U_{iso}*/U_{eq}
O1	0.11169 (8)	0.35585 (8)	0.52445 (6)	0.02229 (17)
O2	0.49733 (8)	0.39415 (8)	0.58292 (6)	0.02091 (16)
N1	−0.09947 (10)	0.21060 (9)	0.09622 (7)	0.02157 (19)
N2	0.25702 (9)	0.46333 (9)	0.45149 (6)	0.01791 (18)
H2N	0.3484 (10)	0.4904 (14)	0.4548 (10)	0.024 (3)*
N3	0.35581 (9)	0.31253 (9)	0.66765 (6)	0.01757 (18)
H3N	0.2664 (11)	0.2971 (14)	0.6716 (11)	0.025 (3)*
N4	0.75967 (10)	0.62970 (10)	0.97336 (7)	0.0225 (2)
C1	−0.14959 (11)	0.32758 (11)	0.12456 (8)	0.0211 (2)
H1	−0.240536	0.343746	0.080891	0.025*
C2	−0.07474 (11)	0.42577 (11)	0.21457 (8)	0.0198 (2)
H2	−0.113267	0.507935	0.231404	0.024*
C3	0.05805 (11)	0.40266 (11)	0.28035 (8)	0.0178 (2)
C4	0.11019 (11)	0.28206 (11)	0.25088 (8)	0.0209 (2)
H4	0.200412	0.262855	0.293315	0.025*
C5	0.02905 (12)	0.18954 (11)	0.15858 (8)	0.0226 (2)
H5	0.066421	0.107775	0.138881	0.027*
C6	0.13776 (11)	0.50952 (11)	0.37960 (8)	0.0190 (2)
H6A	0.178912	0.594422	0.363694	0.023*
H6B	0.064816	0.535030	0.412815	0.023*
C7	0.23279 (11)	0.39410 (10)	0.51848 (7)	0.0168 (2)
C8	0.37639 (11)	0.36670 (10)	0.59305 (7)	0.0165 (2)
C9	0.47933 (11)	0.27763 (11)	0.74404 (8)	0.0198 (2)
H9A	0.539689	0.227162	0.709171	0.024*
H9B	0.439995	0.214321	0.779400	0.024*
C10	0.57768 (11)	0.40374 (10)	0.82273 (7)	0.0179 (2)
C11	0.51872 (12)	0.50271 (12)	0.87410 (9)	0.0261 (2)
H11	0.414595	0.494664	0.858090	0.031*
C12	0.61289 (13)	0.61374 (12)	0.94915 (9)	0.0274 (2)
H12	0.571438	0.680499	0.984407	0.033*
C13	0.81637 (12)	0.53568 (12)	0.92284 (8)	0.0242 (2)
H13	0.920690	0.547791	0.938956	0.029*
C14	0.73011 (12)	0.42117 (12)	0.84793 (8)	0.0224 (2)
H14	0.774771	0.355655	0.814404	0.027*
O3	0.55315 (9)	1.14822 (8)	0.95498 (6)	0.02525 (18)

O4	0.72142 (9)	1.01211 (8)	0.94323 (6)	0.02496 (18)
H4O	0.778 (2)	1.0790 (17)	0.9921 (12)	0.073 (6)*
C15	0.58610 (11)	1.04164 (11)	0.91631 (8)	0.0187 (2)
C16	0.47533 (12)	0.93433 (11)	0.82989 (8)	0.0190 (2)
C17	0.32865 (12)	0.95458 (11)	0.79630 (8)	0.0212 (2)
H17	0.299289	1.032279	0.830770	0.025*
C18	0.22525 (12)	0.86117 (12)	0.71238 (9)	0.0251 (2)
H18	0.125298	0.875244	0.689406	0.030*
C19	0.26769 (13)	0.74743 (12)	0.66210 (9)	0.0277 (2)
H19	0.197060	0.684161	0.604343	0.033*
C20	0.41328 (14)	0.72607 (12)	0.69617 (9)	0.0285 (3)
H20	0.442188	0.648021	0.661755	0.034*
C21	0.51726 (12)	0.81880 (11)	0.78076 (9)	0.0234 (2)
H21	0.616527	0.803107	0.804782	0.028*
O5	−0.16140 (8)	0.74669 (8)	0.22439 (6)	0.02307 (17)
O6	−0.03885 (9)	0.80244 (9)	0.12317 (6)	0.02892 (19)
H6O	−0.1140 (19)	0.747 (2)	0.0769 (14)	0.088 (8)*
C22	−0.05202 (11)	0.80401 (10)	0.21249 (8)	0.0187 (2)
C23	0.08033 (11)	0.88364 (10)	0.30063 (8)	0.0180 (2)
C24	0.20594 (11)	0.94266 (11)	0.28499 (8)	0.0192 (2)
H24	0.209182	0.931865	0.217699	0.023*
C25	0.32654 (12)	1.01739 (11)	0.36799 (8)	0.0220 (2)
H25	0.412647	1.056907	0.357507	0.026*
C26	0.32108 (12)	1.03425 (11)	0.46627 (8)	0.0238 (2)
H26	0.402958	1.086590	0.522807	0.029*
C27	0.19693 (13)	0.97515 (12)	0.48208 (8)	0.0263 (2)
H27	0.193811	0.986854	0.549439	0.032*
C28	0.07667 (12)	0.89864 (12)	0.39969 (8)	0.0234 (2)
H28	−0.007838	0.856648	0.410794	0.028*

Atomic displacement parameters (Å²)

	U^{11}	U^{22}	U^{33}	U^{12}	U^{13}	U^{23}
O1	0.0163 (3)	0.0268 (4)	0.0250 (4)	0.0018 (3)	0.0078 (3)	0.0085 (3)
O2	0.0161 (3)	0.0251 (4)	0.0224 (4)	0.0018 (3)	0.0071 (3)	0.0073 (3)
N1	0.0217 (4)	0.0236 (4)	0.0177 (4)	0.0029 (3)	0.0053 (3)	0.0035 (3)
N2	0.0144 (4)	0.0222 (4)	0.0158 (4)	0.0011 (3)	0.0041 (3)	0.0041 (3)
N3	0.0153 (4)	0.0199 (4)	0.0159 (4)	0.0001 (3)	0.0042 (3)	0.0037 (3)
N4	0.0231 (4)	0.0248 (5)	0.0158 (4)	−0.0006 (4)	0.0035 (3)	0.0036 (3)
C1	0.0189 (5)	0.0246 (5)	0.0190 (5)	0.0039 (4)	0.0040 (4)	0.0072 (4)
C2	0.0193 (5)	0.0200 (5)	0.0205 (5)	0.0045 (4)	0.0064 (4)	0.0055 (4)
C3	0.0171 (5)	0.0206 (5)	0.0168 (5)	0.0014 (4)	0.0068 (4)	0.0058 (4)
C4	0.0189 (5)	0.0245 (5)	0.0188 (5)	0.0056 (4)	0.0050 (4)	0.0058 (4)
C5	0.0241 (5)	0.0230 (5)	0.0207 (5)	0.0072 (4)	0.0072 (4)	0.0039 (4)
C6	0.0187 (5)	0.0203 (5)	0.0171 (5)	0.0039 (4)	0.0045 (4)	0.0046 (4)
C7	0.0166 (5)	0.0166 (4)	0.0151 (4)	0.0012 (4)	0.0048 (4)	0.0008 (4)
C8	0.0166 (4)	0.0147 (4)	0.0154 (4)	0.0005 (3)	0.0041 (4)	0.0005 (4)
C9	0.0199 (5)	0.0194 (5)	0.0178 (5)	0.0021 (4)	0.0033 (4)	0.0051 (4)

C10	0.0193 (5)	0.0200 (5)	0.0138 (4)	0.0020 (4)	0.0038 (4)	0.0061 (4)
C11	0.0174 (5)	0.0309 (6)	0.0248 (5)	0.0033 (4)	0.0044 (4)	−0.0005 (5)
C12	0.0249 (5)	0.0285 (6)	0.0241 (5)	0.0046 (4)	0.0065 (4)	−0.0020 (4)
C13	0.0171 (5)	0.0319 (6)	0.0211 (5)	0.0005 (4)	0.0041 (4)	0.0058 (4)
C14	0.0213 (5)	0.0258 (5)	0.0199 (5)	0.0044 (4)	0.0077 (4)	0.0035 (4)
O3	0.0264 (4)	0.0233 (4)	0.0216 (4)	0.0062 (3)	0.0047 (3)	−0.0006 (3)
O4	0.0220 (4)	0.0262 (4)	0.0213 (4)	0.0050 (3)	0.0038 (3)	−0.0017 (3)
C15	0.0226 (5)	0.0211 (5)	0.0139 (4)	0.0036 (4)	0.0071 (4)	0.0057 (4)
C16	0.0239 (5)	0.0191 (5)	0.0151 (5)	0.0011 (4)	0.0077 (4)	0.0062 (4)
C17	0.0250 (5)	0.0207 (5)	0.0196 (5)	0.0028 (4)	0.0091 (4)	0.0067 (4)
C18	0.0233 (5)	0.0277 (6)	0.0231 (5)	−0.0008 (4)	0.0054 (4)	0.0095 (4)
C19	0.0312 (6)	0.0246 (5)	0.0219 (5)	−0.0066 (4)	0.0061 (4)	0.0030 (4)
C20	0.0346 (6)	0.0211 (5)	0.0271 (6)	−0.0005 (5)	0.0121 (5)	−0.0009 (4)
C21	0.0249 (5)	0.0216 (5)	0.0238 (5)	0.0025 (4)	0.0096 (4)	0.0042 (4)
O5	0.0201 (4)	0.0254 (4)	0.0238 (4)	0.0009 (3)	0.0082 (3)	0.0061 (3)
O6	0.0266 (4)	0.0374 (5)	0.0158 (4)	−0.0093 (3)	0.0058 (3)	−0.0004 (3)
C22	0.0203 (5)	0.0175 (5)	0.0187 (5)	0.0035 (4)	0.0070 (4)	0.0045 (4)
C23	0.0203 (5)	0.0158 (4)	0.0174 (5)	0.0041 (4)	0.0055 (4)	0.0038 (4)
C24	0.0216 (5)	0.0196 (5)	0.0171 (5)	0.0048 (4)	0.0067 (4)	0.0049 (4)
C25	0.0192 (5)	0.0218 (5)	0.0233 (5)	0.0023 (4)	0.0053 (4)	0.0050 (4)
C26	0.0234 (5)	0.0226 (5)	0.0194 (5)	0.0054 (4)	0.0010 (4)	0.0011 (4)
C27	0.0315 (6)	0.0310 (6)	0.0156 (5)	0.0068 (5)	0.0072 (4)	0.0042 (4)
C28	0.0251 (5)	0.0267 (5)	0.0205 (5)	0.0034 (4)	0.0102 (4)	0.0066 (4)

Geometric parameters (Å, º)

O1—C7	1.2270 (12)	C13—H13	0.9500
O2—C8	1.2312 (12)	C14—H14	0.9500
N1—C5	1.3395 (14)	O3—C15	1.2162 (13)
N1—C1	1.3421 (14)	O4—C15	1.3197 (13)
N2—C7	1.3336 (13)	O4—H4O	0.860 (10)
N2—C6	1.4538 (13)	C15—C16	1.4980 (14)
N2—H2N	0.881 (9)	C16—C21	1.3902 (15)
N3—C8	1.3298 (13)	C16—C17	1.3929 (15)
N3—C9	1.4570 (13)	C17—C18	1.3895 (15)
N3—H3N	0.883 (9)	C17—H17	0.9500
N4—C12	1.3346 (15)	C18—C19	1.3867 (17)
N4—C13	1.3338 (15)	C18—H18	0.9500
C1—C2	1.3845 (15)	C19—C20	1.3869 (18)
C1—H1	0.9500	C19—H19	0.9500
C2—C3	1.3968 (14)	C20—C21	1.3935 (16)
C2—H2	0.9500	C20—H20	0.9500
C3—C4	1.3869 (15)	C21—H21	0.9500
C3—C6	1.5157 (14)	O5—C22	1.2237 (13)
C4—C5	1.3906 (15)	O6—C22	1.3084 (13)
C4—H4	0.9500	O6—H6O	0.865 (10)
C5—H5	0.9500	C22—C23	1.4991 (14)
C6—H6A	0.9900	C23—C24	1.3932 (15)

C6—H6B	0.9900	C23—C28	1.3955 (15)
C7—C8	1.5402 (14)	C24—C25	1.3904 (15)
C9—C10	1.5139 (14)	C24—H24	0.9500
C9—H9A	0.9900	C25—C26	1.3893 (16)
C9—H9B	0.9900	C25—H25	0.9500
C10—C11	1.3861 (15)	C26—C27	1.3824 (17)
C10—C14	1.3857 (15)	C26—H26	0.9500
C11—C12	1.3894 (16)	C27—C28	1.3899 (16)
C11—H11	0.9500	C27—H27	0.9500
C12—H12	0.9500	C28—H28	0.9500
C13—C14	1.3857 (15)		

C5—N1—C1	117.75 (9)	N4—C13—C14	123.03 (10)
C7—N2—C6	121.82 (9)	N4—C13—H13	118.5
C7—N2—H2N	119.7 (9)	C14—C13—H13	118.5
C6—N2—H2N	118.1 (9)	C13—C14—C10	118.93 (10)
C8—N3—C9	120.98 (9)	C13—C14—H14	120.5
C8—N3—H3N	120.2 (9)	C10—C14—H14	120.5
C9—N3—H3N	118.8 (9)	C15—O4—H4O	108.5 (15)
C12—N4—C13	118.30 (9)	O3—C15—O4	123.81 (9)
N1—C1—C2	122.96 (10)	O3—C15—C16	122.06 (10)
N1—C1—H1	118.5	O4—C15—C16	114.08 (9)
C2—C1—H1	118.5	C21—C16—C17	119.87 (10)
C1—C2—C3	119.25 (10)	C21—C16—C15	121.37 (10)
C1—C2—H2	120.4	C17—C16—C15	118.72 (9)
C3—C2—H2	120.4	C16—C17—C18	120.01 (10)
C4—C3—C2	117.79 (9)	C16—C17—H17	120.0
C4—C3—C6	123.35 (9)	C18—C17—H17	120.0
C2—C3—C6	118.85 (9)	C19—C18—C17	120.12 (11)
C3—C4—C5	119.32 (10)	C19—C18—H18	119.9
C3—C4—H4	120.3	C17—C18—H18	119.9
C5—C4—H4	120.3	C18—C19—C20	119.98 (10)
N1—C5—C4	122.91 (10)	C18—C19—H19	120.0
N1—C5—H5	118.5	C20—C19—H19	120.0
C4—C5—H5	118.5	C19—C20—C21	120.18 (11)
N2—C6—C3	114.41 (8)	C19—C20—H20	119.9
N2—C6—H6A	108.7	C21—C20—H20	119.9
C3—C6—H6A	108.7	C16—C21—C20	119.82 (11)
N2—C6—H6B	108.7	C16—C21—H21	120.1
C3—C6—H6B	108.7	C20—C21—H21	120.1
H6A—C6—H6B	107.6	C22—O6—H6O	108.4 (17)
O1—C7—N2	125.93 (9)	O5—C22—O6	123.94 (9)
O1—C7—C8	121.14 (9)	O5—C22—C23	122.33 (9)
N2—C7—C8	112.92 (8)	O6—C22—C23	113.73 (9)
O2—C8—N3	124.54 (9)	C24—C23—C28	119.83 (9)
O2—C8—C7	121.86 (9)	C24—C23—C22	121.07 (9)
N3—C8—C7	113.60 (9)	C28—C23—C22	119.10 (9)
N3—C9—C10	113.22 (8)	C25—C24—C23	119.91 (10)

N3—C9—H9A	108.9	C25—C24—H24	120.0
C10—C9—H9A	108.9	C23—C24—H24	120.0
N3—C9—H9B	108.9	C26—C25—C24	119.98 (10)
C10—C9—H9B	108.9	C26—C25—H25	120.0
H9A—C9—H9B	107.7	C24—C25—H25	120.0
C11—C10—C14	117.99 (9)	C27—C26—C25	120.23 (10)
C11—C10—C9	121.18 (9)	C27—C26—H26	119.9
C14—C10—C9	120.79 (9)	C25—C26—H26	119.9
C10—C11—C12	119.57 (10)	C26—C27—C28	120.18 (10)
C10—C11—H11	120.2	C26—C27—H27	119.9
C12—C11—H11	120.2	C28—C27—H27	119.9
N4—C12—C11	122.16 (11)	C27—C28—C23	119.85 (10)
N4—C12—H12	118.9	C27—C28—H28	120.1
C11—C12—H12	118.9	C23—C28—H28	120.1

C5—N1—C1—C2	−0.12 (16)	N4—C13—C14—C10	1.01 (17)
N1—C1—C2—C3	−0.91 (16)	C11—C10—C14—C13	0.07 (16)
C1—C2—C3—C4	1.13 (15)	C9—C10—C14—C13	−177.84 (10)
C1—C2—C3—C6	−178.91 (9)	O3—C15—C16—C21	174.45 (10)
C2—C3—C4—C5	−0.39 (15)	O4—C15—C16—C21	−3.20 (14)
C6—C3—C4—C5	179.65 (10)	O3—C15—C16—C17	−3.13 (15)
C1—N1—C5—C4	0.91 (16)	O4—C15—C16—C17	179.22 (9)
C3—C4—C5—N1	−0.66 (17)	C21—C16—C17—C18	−1.48 (15)
C7—N2—C6—C3	−87.36 (12)	C15—C16—C17—C18	176.13 (9)
C4—C3—C6—N2	−12.00 (14)	C16—C17—C18—C19	0.20 (16)
C2—C3—C6—N2	168.05 (9)	C17—C18—C19—C20	0.61 (17)
C6—N2—C7—O1	3.86 (16)	C18—C19—C20—C21	−0.12 (18)
C6—N2—C7—C8	−175.03 (8)	C17—C16—C21—C20	1.96 (16)
C9—N3—C8—O2	−1.50 (15)	C15—C16—C21—C20	−175.59 (10)
C9—N3—C8—C7	178.88 (8)	C19—C20—C21—C16	−1.17 (17)
O1—C7—C8—O2	173.94 (9)	O5—C22—C23—C24	177.14 (10)
N2—C7—C8—O2	−7.10 (13)	O6—C22—C23—C24	−3.01 (14)
O1—C7—C8—N3	−6.43 (13)	O5—C22—C23—C28	−2.98 (16)
N2—C7—C8—N3	172.52 (8)	O6—C22—C23—C28	176.87 (10)
C8—N3—C9—C10	75.45 (12)	C28—C23—C24—C25	−0.63 (15)
N3—C9—C10—C11	50.59 (14)	C22—C23—C24—C25	179.25 (9)
N3—C9—C10—C14	−131.57 (10)	C23—C24—C25—C26	−0.63 (16)
C14—C10—C11—C12	−0.84 (17)	C24—C25—C26—C27	1.00 (16)
C9—C10—C11—C12	177.05 (10)	C25—C26—C27—C28	−0.10 (17)
C13—N4—C12—C11	0.40 (18)	C26—C27—C28—C23	−1.16 (17)
C10—C11—C12—N4	0.64 (19)	C24—C23—C28—C27	1.52 (16)
C12—N4—C13—C14	−1.24 (17)	C22—C23—C28—C27	−178.36 (10)

Hydrogen-bond geometry (Å, º)

D—H···*A*	*D*—H	H···*A*	*D*···*A*	*D*—H···*A*
N2—H2*N*···O2	0.88 (1)	2.36 (1)	2.7192 (12)	105 (1)
N3—H3*N*···O1	0.88 (1)	2.36 (1)	2.7154 (12)	104 (1)

O4—H4*O*···N1^{i}	0.86 (2)	1.78 (2)	2.6366 (12)	177 (2)
O6—H6*O*···N4^{ii}	0.86 (2)	1.72 (2)	2.5731 (13)	169 (2)
N2—H2*N*···O2^{iii}	0.88 (1)	2.05 (1)	2.8618 (12)	152 (1)
N3—H3*N*···O5^{iv}	0.88 (1)	2.12 (1)	2.8516 (12)	140 (1)
C1—H1···O3^{v}	0.95	2.58	3.2009 (14)	124
C2—H2···O5	0.95	2.47	3.3602 (14)	155
C6—H6*B*···O1^{iv}	0.99	2.41	3.3826 (14)	166
C12—H12···O3^{vi}	0.95	2.36	3.3025 (15)	171

Symmetry codes: (i) *x*+1, *y*+1, *z*+1; (ii) *x*−1, *y*, *z*−1; (iii) −*x*+1, −*y*+1, −*z*+1; (iv) −*x*, −*y*+1, −*z*+1; (v) *x*−1, *y*−1, *z*−1; (vi) −*x*+1, −*y*+2, −*z*+2.